Soft Matter

PAPER

View Article Online
View Journal | View Issue

Cite this: *Soft Matter*, 2023, **19**, 7663

Electrostatic force on a spherical particle confined between two planar surfaces†

Zhanwen Wang, [a] Michael J. Miksis[b] and Petia M. Vlahovska *[b]

Received 16th July 2023,
Accepted 13th September 2023

DOI: 10.1039/d3sm00934c

rsc.li/soft-matter-journal

A charge-free particle in a uniform electric field experiences no net force in an unbounded domain. A boundary, however, breaks the symmetry and the particle can be attracted or repelled to it, depending on the applied field direction [Z. Wang *et al.*, *Phys. Rev. E*, 2022, **106**, 034607]. Here, we investigate the effect of a second boundary because of its common occurrence in practical applications. We consider a spherical particle suspended between two parallel walls and subjected to a uniform electric field, applied in a direction either normal or tangential to the surfaces. All media are modeled as leaky dielectrics, thus allowing for the accumulation of free charge at interfaces, while bulk media remain charge-free. The Laplace equation for the electric potential is solved using a multipole expansion and the boundaries are accounted for by a set of images. The results show that in the case of a normal electric field, which corresponds to a particle between two electrodes, the force is always attractive to the nearer boundary and, in general, weaker that the case of only one wall. Intriguingly, for a given particle–wall separation we find that the force may vary nonmonotonically with confinement and its magnitude may exceed the one-wall value. In the case of tangential electric field, which corresponds to a particle between insulating boundaries, the force follows the same trends but it is always repulsive.

1 Introduction

Electric fields are commonly used to manipulate colloidal particles[1–6] and droplets.[7,8] Electric fields drive electrohydrodynamic flows that assemble colloidal crystals on electrodes[9] and have also become a popular means to energize and create self-propelled particles[10–14] due to field-induced charge electrophoresis[15–17] or torque due to the Quincke effect, which drives colloids to roll on a surface.[18–23] Electric fields enable active control of droplets in microfluidics.[24–26] In these applications particles are often confined by electrodes or channels, and the electrostatic force (and torque) exerted on the particle is significantly influenced by the bounding surfaces.

The force on an spherical colloid near a planar boundary has been mostly analyzed in the two limiting cases of a conducting or an insulating particle. The surface of a conducting particle is equipotential, and consequently, the electric field inside vanishes. The net charge and force on a spherical particle are calculated using the method of images[27,28] or the equivalent problem of two spheres in a uniform electric field.[29] If the particle is a perfect insulator and charge-free, the boundary condition on the particle-medium interface are continuity of the electric potential and the displacement field. The electrostatic force has been obtained either in terms of series expansion in eigenfunctions of the Laplace equation in bispherical coordinate system,[30–34] or from a multipole-moment theory for the pair-wise dielectrophoretic interactions of dielectric spheres.[35,36] Real materials are, however, rarely perfectly insulating. Even a weak conduction leads to the accumulation of free charges at interfaces,[37] which can profoundly affect the particle electrostatics. In the case where particle and suspending media are leaky dielectrics, the appropriate boundary conditions at interfaces are continuity the normal electric current rather than the displacement field.[38] The discontinuity of the latter determines the induced free charge distributed along the interface (with net charge being zero). The bulk media remain charge-free and the electrostatic potential is a solution of the Laplace equation.

Recently, this leaky dielectric model was used to analyze the spherical particle–wall interactions for particle and suspending media with arbitrary conductivities.[39] Electric fields applied both normal to an electrode or tangential to an insulating boundary were considered and the force calculated for arbitrary particle separations. Here, we consider the effect of a second, parallel boundary on the electrostatic force on the particle. This paper is organized as follows. The problem is formulated in Section 2. In Section 3, the solution methodology using the

[a] *Theoretical and Applied Mechanics Program, Northwestern University, Evanston, IL 60208, USA*
[b] *Engineering Sciences and Applied Mathematics, Northwestern University, Evanston, IL 60208, USA. E-mail: petia.vlahovska@northwestern.edu*

† Electronic supplementary information (ESI) available. See DOI: https://doi.org/10.1039/d3sm00934c

method of images and the mulitpole expansion is presented, which is a generalization of the approach developed by Washizu and Jones[35] for two identical particles in a uniform electric field. First, the solution of the electric field is expressed in terms of a series of Legendre polynomials, and an algorithm to determine the expansion coefficients is developed. Then the force on the particle is calculated. In Section 4, we explore the force dependence on confinement and media electric properties.

2 Problem formulation

Let us consider a spherical particle with radius a, conductivity σ_1 and permittivity ε_1, suspended in a medium with conductivity σ_2 and permittivity ε_2 between two parallel planar walls. A Cartesian coordinates system $(\tilde{x},\tilde{y},\tilde{z})$ is centered along the lower wall below the particle. The particle has zero net charge. The distance between the walls is H. The particle center is located at $(\tilde{x},\tilde{y},\tilde{z}) = (0,0,h)$. The applied electric field, with magnitude E_0, is either normal or tangential to the bounding walls (Fig. 1). Hereafter, we rescale all variables by E_0 and a. The dimensionless Cartesian coordinates are $(x,y,z) = (\tilde{x}/a,\tilde{y}/a,\tilde{z}/a)$. The rescaling introduces three dimensionless geometry parameters: the dimensionless height of the particle center above the bottom wall, $\delta_c = h/a$, the dimensionless gap between the particle surface and bottom wall, $\delta_p = \delta_c - 1$, and the dimensionless distance between two walls, $\delta_w = H/a$.

To solve for the electric field and find the electrostatic force on the particle, we adopt the leaky dielectric model,[37] which assumes charge-free bulk media and attributes the space charge in the diffuse layers near boundaries to the interface. The model has been shown to be a good approximation of the full electrokinetic equations in the case of thin Debye layers.[40–45] Accordingly, the dimensionless electric potential inside the particle, Φ_1, and in the medium, Φ_2, satisfy the Laplace's equation

$$\nabla^2\Phi_i = 0, \quad i = 1, 2. \tag{1}$$

The electric potential and normal electric current are continuous. The boundary conditions on the at $r = 1$ read

$$\Phi_1 = \Phi_2,\ \chi\mathbf{n}\cdot\mathbf{E}_1 = \mathbf{n}\cdot\mathbf{E}_2, \tag{2}$$

where $\mathbf{n}$ is the outward-pointing normal to the interface and χ is the conductivity ratio, $\chi = \sigma_1/\sigma_2$. The continuity of the normal electric current implies discontinuous displacement electric field; its jump defines the interfacial charge. Note that the interfacial charge distribution is nonuniform (and in a uniform applied electric field it has a dipolar character), and the net charge is zero. The boundary condition on the confining walls depends on the direction of applied electric field. In the case of a normal electric field, the two plane walls are conducting and equipotential:

$$\Phi_2 = \begin{cases} -\delta_w & \text{at } z = \delta_w, \\ 0 & \text{at } z = 0. \end{cases} \tag{3}$$

In the case of a tangentially applied electric field, the walls are insulating, and the normal electric current vanishes

$$\frac{\partial\Phi_2}{\partial z} = 0 \text{ at } z = 0, \delta_w. \tag{4}$$

Let us introduce dimensionless disturbance field $\hat{\Phi}_1$ and $\hat{\Phi}_2$,

$$\Phi_i = \hat{\Phi}_i - x_\alpha, \tag{5}$$

where x_α is the direction of applied electric field, $x_\alpha = z$ for the normal electric field and $x_\alpha = x$ for the tangential electric field. The disturbance fields satisfy Laplace's equation, with boundary conditions at the particle-medium interface

$$\hat{\Phi}_1 = \hat{\Phi}_2,\ \chi\frac{\partial\hat{\Phi}_1}{\partial n} - \frac{\partial\hat{\Phi}_2}{\partial n} = (\chi - 1)\frac{\partial x_\alpha}{\partial n}. \tag{6}$$

and homogenous boundary conditions on the two bounding walls

$$\begin{cases} \hat{\Phi}_2 = 0 & \text{Normal electric field}, \\ \partial\hat{\Phi}_2/\partial z = 0 & \text{Tangential electric field}. \end{cases} \tag{7}$$

3 Solution

3.1 Electric field

Following Washizu and Jones,[35] the perturbation in the applied electric field due to a particle confined between two planar surfaces can be represented as a sum of multipoles of strength $B_{n,m}$ placed at the particle center and image multipoles $M_{n,m}$ that account for the boundary effects (see ESI,† for details)

$$\hat{\Phi}_2 = \sum_{n=m}^{\infty}\left(\frac{B_{n,m}}{r^{n+1}} + M_{n,m}r^n\right)P_n^m(\cos\theta)\cos(m\phi), \tag{8}$$

Here $m = 0$ corresponds to the case of a particle between two electrodes (electric field applied normal to the surfaces), while $m = 1$ is the case of a tangentially applied electric field. (r,θ,ϕ) denote spherical coordinates centered at the particle.

The effect of the boundaries is accounted for by the method of images. The two walls require two sets of images: a series of successive images starting with a reflection with respect of the bottom wall, β, and a series of images starting with a reflection by the top wall, γ. For group β, the first image $\beta^{(1)}_{n,m}$ is the mirror image of the original multipole $B_{n,m}$ relative to the bottom wall. The relation between multipole components $\beta^{(i)}_{n,m}$ and $\beta^{(i-1)}_{n,m}$ is given by

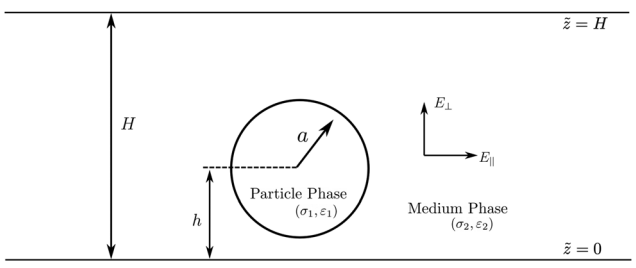

Fig. 1 Sketch of the problem. A cross-section in the $y = 0$ plane is shown.

$$\beta_{j,k}^{(i)} = (-1)^{j+k+1}\beta_{j,k}^{(i-1)}, \quad (9)$$

for the case of the normal electric field and equipotential walls, and

$$\beta_{j,k}^{(i)} = (-1)^{j+k}\beta_{j,k}^{(i-1)}, \quad (10)$$

for the case of tangentially applied electric field and insulating boundaries. The positions of the images in group β is determined successively,

$$z_i = \begin{cases} 2\delta_w - z_{i-1} & i \text{ even} \\ -z_{i-1} & i \text{ odd} \end{cases}$$

Image group γ is constructed using the same procedure, starting with $\gamma_{n,m}^{(1)}$ as the mirror image of $B_{n,m}$ relative to the top wall.

For both cases of the applied electric fields, the location of images are $-\delta_c$, $2k\delta_w \pm \delta_c$, and $-2k\delta_w \pm \delta_c$, $k = 1, 2, 3, \ldots$. Images located at $2k\delta_w + \delta_c$ and $-2k\delta_w + \delta_c$ have all components the same as the original multipole while some of components of images located at $-\delta_c$, $2k\delta_w - \delta_c$, and $-2k\delta_w - \delta_c$ have opposite sign.

The images fields are re-expanded about the particle center, $r = 0$, which yields $M_{n,m}$ as the sum of all their contributions as

$$M_{n,m} = \sum_{l=m}^{\infty} N_{n,l}^{(m)} B_{l,m}. \quad (11)$$

The coefficients $N_{n,l}^{(m)}$ only depend on the geometry parameters δ_c and δ_w (see ESI,† for details of the derivation). In the case of a particle between two electrodes

$$N_{n,l}^{(0)} = \frac{(n+l)!}{l!n!} C_{n,l}, \quad (12)$$

where

$$C_{n,l} = \frac{1}{(-2\delta_c)^{n+l+1}} + \sum_{k=1}^{\infty}\left[\frac{(-1)^l + (-1)^n}{(2k\delta_w)^{n+l+1}} - \frac{1}{(2k\delta_w - 2\delta_c)^{n+l+1}} - \frac{(-1)^{n+l}}{(2k\delta_w + 2\delta_c)^{n+l+1}}\right]. \quad (13)$$

For a tangentially applied electric field

$$N_{n,l}^{(1)} = -\frac{(n+l)!}{(l-1)!(n+1)!} C_{n,l}. \quad (14)$$

Convergence of eqn (8) requires that r is limited by the two walls and the particle, *i.e.*, $1 \le r \le \min[\delta_c, \delta_w - \delta_c]$.

The disturbance field inside the particle is given by the nonsingular (at $r = 0$) solutions of the Laplace equation

$$\hat{\Phi}_1 = \sum_{n=m}^{\infty} A_{n,m} r^n P_n^m(\cos\theta)\cos(m\phi). \quad (15)$$

The next step is to match $\hat{\Phi}_1$ and $\hat{\Phi}_2$ using the boundary conditions at particle-medium interface $r = 1$. Substituting eqn (8) and (15) into the equation for the continuity of electric potential eqn (2), we obtain

$$A_{n,m} = M_{n,m} + B_{n,m}. \quad (16)$$

The continuity of the normal electric current, together with eqn 11 and (16), leads to a set of algebraic equations to be solved for the multipoles $B_{n,m}$, $n = 1, 2\ldots$,

$$\sum_{l=m}^{\infty}\left[(\chi-1)nN_{n,l}^{(m)} + (n\chi + n + 1)\delta_{nl}\right]B_{l,m} = (\chi-1)G_{n,m}, \quad (17)$$

where δ_{nl} denotes the Kronecker delta and $G_{n,m}$ comes from the eigenfunction expansion of $\partial x_\alpha/\partial n$,

$$\left.\frac{\partial x_\alpha}{\partial n}\right|_{r=1} = \sum_{n=m}^{\infty} G_{n,m} P_n^m(\cos\theta)\cos(m\phi). \quad (18)$$

In the case of a normal electric field, $x_\alpha = z = \delta_c + r\cos\theta$, $\partial z/\partial r = \cos\theta = P_1(\cos\theta)$. From eqn (18), we obtain $G_{n,0} = \delta_{n1}$. In the case of tangentially applied electric field, $x_\alpha = x = r\sin\theta\cos\phi$. Since $P_1^{\,1}(\cos\theta) = -\sin\theta$, the coefficients $G_{n,1} = -\delta_{n1}$.

3.2 Electrostatic force on the particle

The force is calculated using the approach developed by Washizu and Jones.[46] The particle disturbance to the applied field is modeled as due to an effective charge distributed on the particle surface

$$\sigma_t = -\sum_{n=m}^{\infty} K_n M'_{n,m} P_n^m(\cos\theta)\cos(m\phi), \quad (19)$$

where

$$K_n = \frac{n(2n+1)(\chi-1)}{n\chi + n + 1}. \quad (20)$$

$M'_{n,m} = M_{n,m} - H_{n,m}$ with $H_{n,m}$ is obtained from expanding x_α,

$$x_\alpha = \sum_{n=m}^{\infty} H_{n,m} r^n P_n^m(\cos\theta)\cos(m\phi). \quad (21)$$

Accordingly, the dimensionless force, denoted as force coefficient $C_f = F_z/(\varepsilon_2 E_0{}^2 a^2)$, on the particle is

$$C_f = \oint_{r=1} \sigma_t\left(-\frac{\partial \Phi_{ext}}{\partial z}\right)\mathrm{d}S, \quad (22)$$

where Φ_{ext} is the electric potential due to the applied field and all the images,

$$\Phi_{ext} = -x_\alpha + \sum_{n=m}^{\infty} M_{n,m} r^n P_n^m(\cos\theta)\cos(m\phi).$$

Taking the derivative with respect to z yields

$$\frac{\partial \Phi_{ext}}{\partial z} = \sum_{n=m}^{\infty} M'_{n,m}(n+m) r^{n-1} P_{n-1}^m(\cos\theta)\cos(m\phi).$$

Substituting into eqn (22) leads to

$$C_f = \sum_{n=m}^{\infty}\sum_{k=m}^{\infty}(k+m) K_n M'_{n,m} M'_{k,m} \times \oint_{r=1} P_n^m(\cos\theta)\cos(m\phi) P_{k-1}^m(\cos\theta)\cos(m\phi)\mathrm{d}S \quad (23)$$

The integral is evaluated using the orthogonality of the

associated Legendre polynomials,

$$\oint_{r=1} P_{n_1}^m(\cos\theta)\cos(m\phi)P_{n_2}^m(\cos\theta)\cos(m\phi)\mathrm{d}S = \begin{cases} \dfrac{4\pi}{2n+1}\delta_{n_1n_2} & m=0, \\ \dfrac{2\pi(n+m)!}{(2n+1)(n-m)!}\delta_{n_1n_2} & m\neq 0. \end{cases} \quad (24)$$

3.2.1 Normal electric field. In the case of an electric field applied perpendicularly to the walls, the problem is axisymmetric, $m = 0$, and the force is

$$C_f = 4\pi\sum_{n=1}^{\infty} K_n \frac{n+1}{2n+1} M'_{n,0} M'_{n+1,0}. \quad (25)$$

where coefficients $M'_{n,0}$ are

$$M'_{n,0} = \begin{cases} M_{1,0} - 1 & n = 1 \\ M_{n,0} & n = 2, 3, \ldots \end{cases}. \quad (26)$$

Note that if the particle is a perfect conductor, it charges when in contact with the electrode. The calculation of the force in this case is presented in the Appendix A.

3.2.2 Tangential electric field. In the case of a tangentially applied electric field in the x direction. $m = 1$. Using eqn (22), we find

$$C_f = 2\pi\sum_{n=1}^{\infty} K_n \frac{n(n+1)(n+2)}{2n+1} M'_{n,1} M'_{n+1,1}, \quad (27)$$

where coefficients $M'_{n,1}$ are

$$M'_{n,1} = \begin{cases} M_{1,1} + 1 & n = 1, \\ M_{n,1} & n = 2, 3, \ldots \end{cases}. \quad (28)$$

4 Results and discussion

In this section, we investigate the particle–wall interaction at different confinement, and different material properties of the particle and the suspending media. Specifically, we analyze the dependence of the force on the

- Dimensionless distance between the two walls, $\delta_w = H/a$, $\delta_p + 2 < \delta_w < \infty$
- Dimensionless gap between the particle surface and the bottom wall, $\delta_p = (h - a)/a$, $0 < \delta_p < \delta_w - 2$,
- Conductivity ratio, $\chi = \sigma_1/\sigma_2$.

All calculations are done with sums truncated at 50 terms (eqn (25) and (27)), which is sufficient to achieve a converged result (see ESI,† for details of the convergence tests).

4.1 Normal electric field

Fig. 2 shows the variation of the force with the particle-electrode gap at a given separation between the electrodes. The force coefficient C_f, defined as the interaction force normalized by $\varepsilon_2 E_0^2 a^2$, is plotted as a function of the particle to bottom-electrode gap, δ_p for different electrode distance, δ_w. Fig. 2(b) replots the data as a function of $(\delta_p + 1)/\delta_w - 1/2$, which is zero when the particle center is at the midplane between the electrodes. The magnitude of force is symmetric about the midplane while the direction changes sign since the particle is attracted to the nearer electrode.

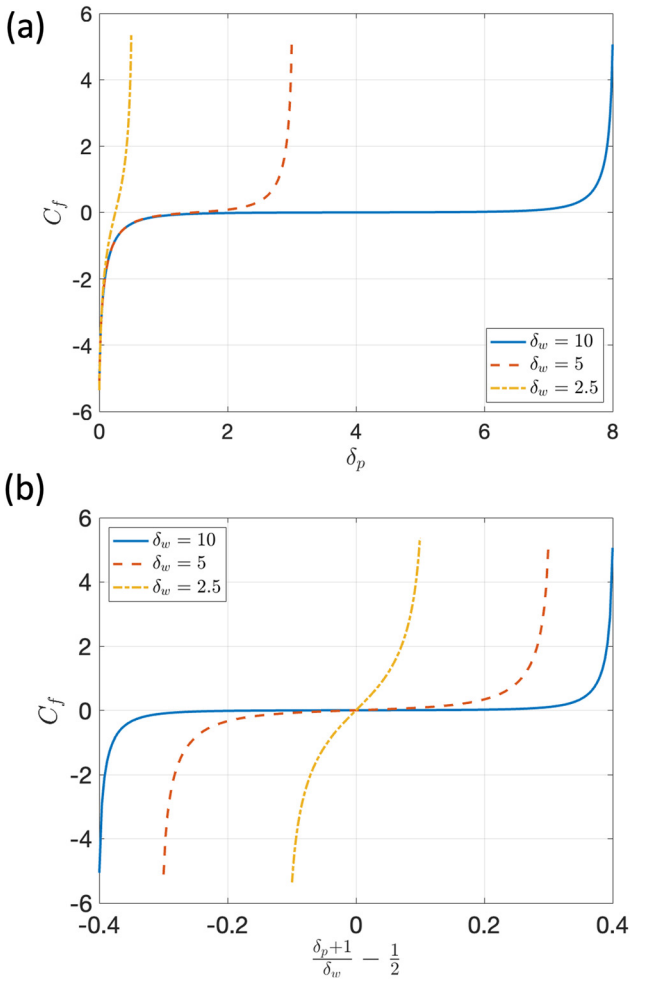

Fig. 2 Particle between two electrodes: force coefficient $C_f = F_z/(\varepsilon_2 E_0^2 a^2)$ as a function of the gap between the particle and the bottom electrode, δ_p, and different electrode separations, δ_w (a). Panel (b) replots the data as a function of $(\delta_p + 1)/\delta_w - 1/2$, the deviation of the particle center from the midplane. Conductivity ratio is $\chi = 5$.

Fig. 3 illustrates the effect of the conductivity ratio χ on the force. Since χ varies between 0, for an insulating particle, to ∞ for a perfectly conducting particle, we introduce the conductivity mismatch $\beta_{12} = (\chi - 1)/(\chi + 1)$ which has a finite range from -1 to 1, which is more convenient for plotting. The force behavior is similar to the one-electrode solution,[39] which means that introduction of the top electrode does not change the problem qualitatively. The presence of the top electrode only decreases the magnitude of the force, and weakens the attraction by the nearer electrode.

Intriguingly, we find that the force may vary non-monotonically with the confinement δ_w for a fixed particle-electrode gap, see Fig. 4. At large distance between the electrodes, $\delta_w \gg 1$,

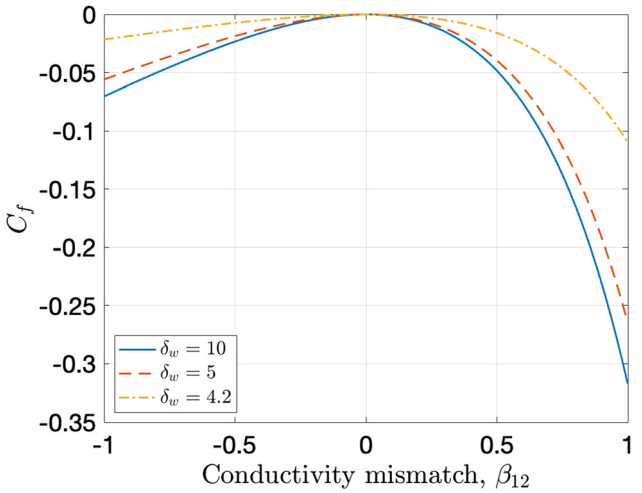

Fig. 3 Particle between two electrodes: force coefficient $C_f = F_z/(\varepsilon_2 E_0^2 a^2)$ as a function of the conductivity mismatch $\beta_{12} = (\chi - 1)/(\chi + 1)$ for fixed $\delta_p = 1$ and various δ_w. $\beta_{12} = 1$ corresponds to a perfectly conducting particle, while $\beta_{12} = -1$ corresponds to a perfectly insulating particle.

the two-electrode solution approaches the one-wall result.[39] At the minimum value of δ_w in the figure, $2(\delta_p + 1)$, where the particle center is at the mid-plane between the electrodes, the force vanishes. As the confinement decreases, however, the magnitude of the force coefficient C_f behaves differently depending on the conductivity ratio χ. When the particle is more conducting than the suspending medium, $\chi > 1$, see Fig. 4(a), the force magnitude passes through a maximum value (a "peak") that exceeds the one-wall solution. In the case of $\chi < 1$, Fig. 4(b), the magnitude of C_f monotonically decreases to zero as the electrode separation decreases. We also compare the exact two-wall solution with the approximate superposition solution, which is the sum of two one-wall solutions with dimensionless particle surface to plane wall gaps δ_p and $\delta_w - \delta_p - 2$, respectively. In general, the superposition solution is a good approximation of the two-wall problem, especially in the case $\chi < 1$. However, it can not predict the "peak" since two the electrodes attract the particle in opposite directions.

A contour plot of the "peak"' magnitude, defined as the maximum difference of the force magnitude between the two-wall and one-wall solutions scaled by the one-wall solution, as a function of particle–wall gap and conductivity ratio, is shown in Fig. 5. The "peak" is most pronounced when the conductivity mismatch is large, $\chi \gg 1$ (conducting particle) and the particle is close to the bottom wall, $\delta_p \ll 1$.

The non-monotonic behavior of the force arises from the competing interactions of the images $\beta^{(1)}_{n,m}$ and $\gamma^{(1)}_{n,m}$ and the particle multipoles $B_{n,m}$. In the case of $\delta_w \gg \delta_p \gg 1$, the origin of the peak can be illuminated by considering the interactions between the leading order multipoles, the particle dipole $B_{1,0}$ and its two closest image dipoles $\beta^{(1)}_{1,0}$ and $\gamma^{(1)}_{1,0}$, which all have the same magnitude $B_{1,0} = \beta^{(1)}_{1,0} = \gamma^{(1)}_{1,0}$. The force is then

$$C_f = \frac{3\pi}{2} B_{1,0}{}^2 \left[\frac{1}{(\delta_p + 1 - \delta_w)^4} - \frac{1}{(\delta_p + 1)^4} \right], \qquad (29)$$

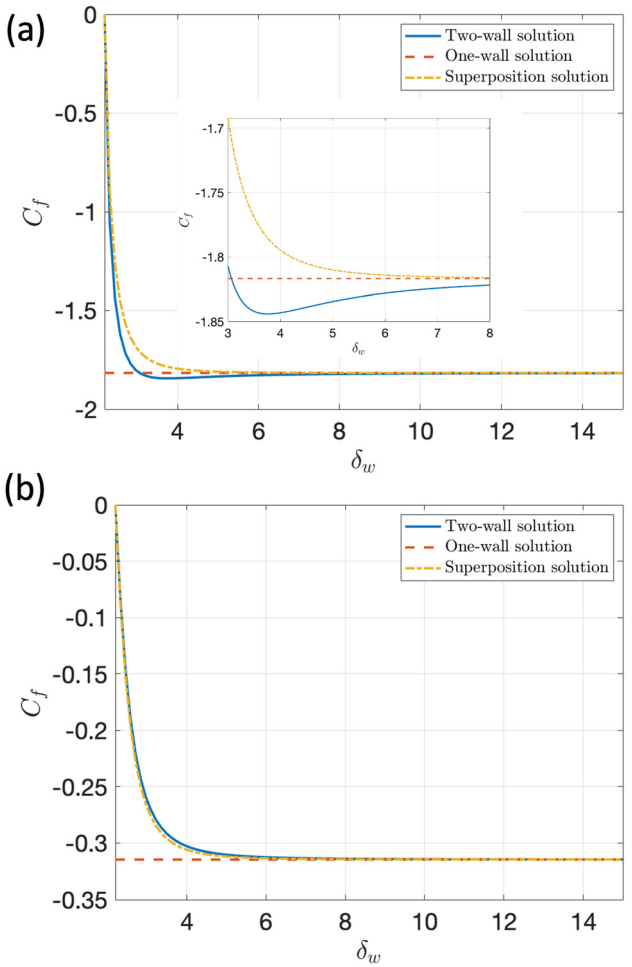

Fig. 4 Particle between two electrodes: force coefficient C_f as a function of the dimensionless separation between two electrodes δ_w and fixed particle-electrode gap. The superposition solution stands for the sum of two opposite one-wall solutions. (a) $\delta_p = 0.1$ and $\chi = 5$ (b) $\delta_p = 0.1$ and $\chi = 0.2$.

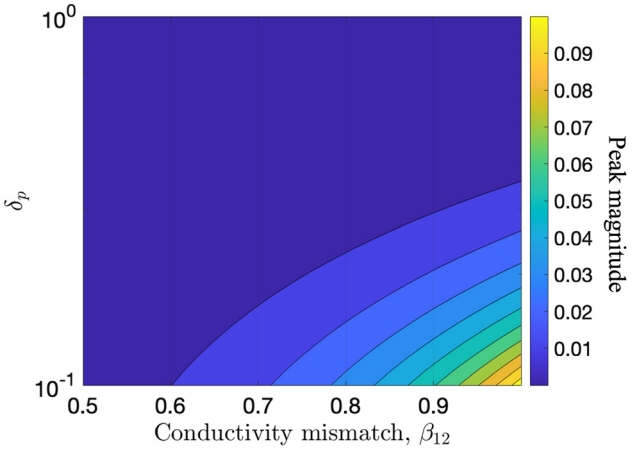

Fig. 5 Particle between two electrodes: peak magnitude of the force coefficient, scaled by the one wall solution, as a function of the conductivity mismatch $\beta_{12} = (\chi - 1)/(\chi + 1)$ and δ_p.

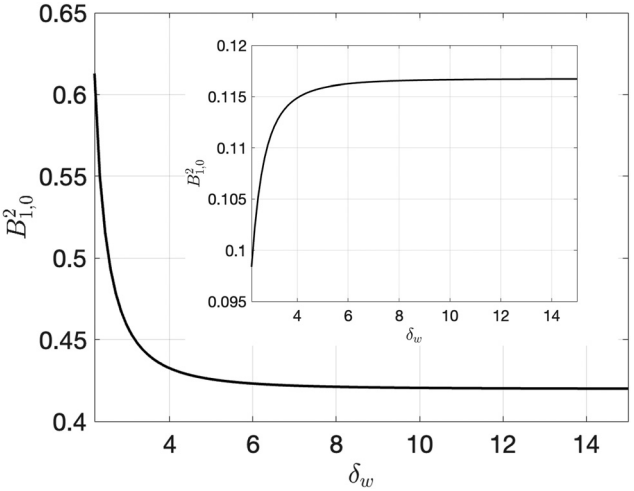

Fig. 6 Normal field: the square of dimensionless dipole, $B_{1,0}$, as a function of dimensionless confinement δ_w for χ = 5 and δ_p = 0.1. Inset: χ = 0.2, δ_p = 0.1.

When the electrode separation is large, $\delta_w \gg 1$, the second term on the right hand side of Eqn 29 dominates. In the case of $\chi > 1$, ${B_{1,0}}^2$ increases as the gap between two walls decreases, see Fig. 6, which increases the force magnitude (the force on Fig. 4 a becomes more negative). When $\delta_w \sim O(1)$, the first term becomes the dominant contribution thereby reversing the trend. Eventually, the magnitude of force becomes zero when $\delta_w = 2(\delta_p + 1)$, when the particle center reaches the mid-plane between the electrodes. However, if $\chi < 1$, the dipole magnitude decreases with decreasing δ_w. Thus, both terms on the right hand side are monotonically decreasing, which leads to the monotonic decreasing behavior in Fig. 4(b). A more precise argument can be made based on the asymptotic behavior at large δ_w, see eqn (35)–(39) below.

$$B_{1,0} \sim (B_0)_{1,0} + {\delta_w}^{-3}(B_3)_{1,0}, \tag{30}$$

where $(B_0)_{1,0}$ and $(B_3)_{1,0}$ are

$$(B_0)_{1,0} = \frac{\chi - 1}{\chi + 2}, \quad (B_3)_{1,0} = \zeta(3)\left[(B_0)_{1,0}\right]^2. \tag{31}$$

ζ is the Riemann zeta function.

The "peak" exist only if $dC_f/d\delta_w = 0$. Taking derivative of eqn (29) with respect to δ_w, equating with 0, and rearranging the terms yields the following relation

$$\frac{d{B_{1,0}}^2}{d\delta_w}\frac{1}{(\delta_p+1)^4}\left[\frac{1}{\left(\frac{\delta_w}{\delta_p+1}-1\right)^4}-1\right] = \frac{4{B_{1,0}}^2}{(\delta_w-\delta_p-1)^5}. \tag{32}$$

The right hand side of the above equation is positive. Since $\delta_w > 2(\delta_p + 1)$ for a particle near the bottom electrode, this implies that

$$\frac{d{B_{1,0}}^2}{d\delta_w} = 2B_{1,0}\frac{dB_{1,0}}{d\delta_w} < 0. \tag{33}$$

The dipole $B_{1,0}$ behaves asymptotically as eqn (30). Accordingly,

$$\frac{d{B_{1,0}}^2}{d\delta_w} \sim -\frac{3}{{\delta_w}^4}(B_0)_{1,0}(B_3)_{1,0} = -\frac{3}{{\delta_w}^4}\zeta(3)\left(\frac{\chi-1}{\chi+2}\right)^3, \tag{34}$$

which show that a "peak" arises only if $\chi > 1$ in the case of a normal electric field.

The precise asymptotic behavior of the force for large electrode separations, $\delta_w \gg 1$, is obtained by noting that

$$N_{n,l}^{(m)} = X_{n,l}^{(m)} + {\delta_w}^{-3}Z_{n,l}^{(m)}, \tag{35}$$

where for a particle between two electrodes (m = 0)

$$X_{n,l}^{(0)} = \frac{(n+l)!}{l!n!}(-2\delta_c)^{-(n+l+1)},\ Z_{n,l}^{(0)} = \begin{cases} -\zeta(3) & (n,l) = (1,1), \\ 0 & \text{otherwise.} \end{cases} \tag{36}$$

Consequently, the interaction force on the particle has the following form,

$$\begin{aligned} C_f &\sim C_{f0} + {\delta_w}^{-3}C_{f3}, \\ C_{f0} &= 4\pi\sum_{n=1}^{\infty} K_n\frac{n+1}{2n+1}\left(M_0'\right)_{n,0}\left(M_0'\right)_{n+1,0}, \\ C_{f3} &= 4\pi\sum_{n=1}^{\infty} K_n\frac{n+1}{2n+1}\left[\left(M_0'\right)_{n,0}(M_3)_{n+1,0} + (M_3)_{n,0}\left(M_0'\right)_{n+1,0}\right], \end{aligned} \tag{37}$$

The sign of C_{f3} indicates if the force will behave non-monotonically with δ_w. If negative, the attraction between the particle and the nearer electrode is stronger at large electrode separations. However, the force should vanish when the particle is maximally confined and its center is at the midpoint between the electrodes. The increase in C_f at large δ_w should reverse to decreasing at small δ_w, leading to non-monotonicity. The M coefficients are expanded $M_{n,0} \sim (M_0)_{n,0} + {\delta_w}^{-3}(M_3)_{n,0}$

$$\begin{aligned} (M_0)_{n,0} &= \sum_{l=1}^{\infty} X_{n,l}^{(0)}(B_0)_{l,0} \\ (M_3)_{n,0} &= \sum_{l=1}^{\infty} X_{n,l}^{(0)}(B_3)_{l,0} + \sum_{l=1}^{\infty} Z_{n,l}^{(0)}(B_0)_{l,0} \end{aligned} \tag{38}$$

$(B_0)_{l,m}$ and $(B_3)_{l,m}$ are found from the following equations

$$\begin{aligned} &\sum_{l=1}^{\infty}\left[(\chi-1)nX_{n,l}^{(0)} + (n\chi+n+1)\delta_{nl}\right](B_0)_{l,0} = (\chi-1)G_{n,0}, \\ &\sum_{l=1}^{\infty}\left[(\chi-1)nX_{n,l}^{(0)} + (n\chi+n+1)\delta_{nl}\right] \\ &(B_3)_{l,0} = -(\chi-1)n\sum_{l=1}^{\infty} Z_{n,l}^{(0)}(B_0)_{l,0}. \end{aligned} \tag{39}$$

where n = 1, 2…. This asymptotic solution for the force for large distance between two walls $\delta_w \gg 1$ is detailed in the ESI.† Fig. 7 shows that the asymptotic solution provides a good approximation to the full solution down to $\delta_w \sim 5$.

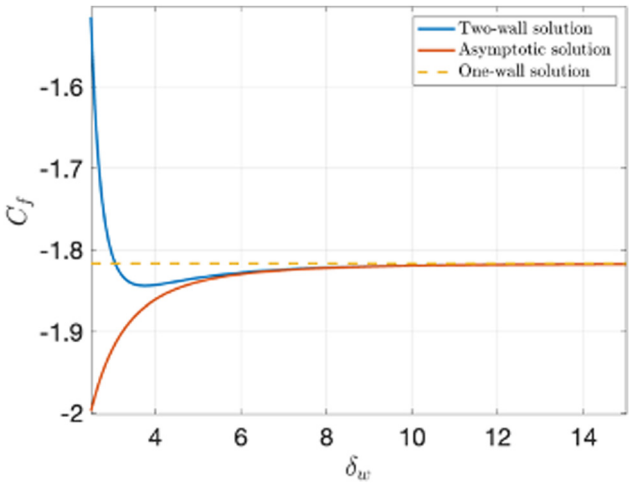

Fig. 7 Normal field: force coefficient C_f as a function of δ_w, the dimensionless gap between two electrodes, compared to the asymptotic solution. δ_p = 0.1, χ = 9.

4.2 Tangential electric field

Fig. 8–13 provide the plots for tangentially applied electric field mirroring Fig. 2–7 for the normal electric field. The trends are the same as the normal electric field, however the interaction is with a reversed sign. The particle is repelled by the nearer wall in the case of tangential electric field since the particle dipole and its images are parallel.

The non-monotonic dependence on the confinement δ_w is also found in the case of tangential electric field. The mechanism is same as the normal electric field (discussed in the previous section). The square of dipole ${B_{1,1}}^2$ increases as the gap between two walls decreases when $\chi < 1$ (see Fig. 11), which contrasts the case of normal electric field. Consequently, the non-monotonic behavior appears when $\chi < 1$ (see Fig. 10(b)). The magnitude of the "peak", which is defined as the maximum difference of the force magnitude between the two-wall and one-wall solutions, is presented in Fig. 12. The "peak" magnitude is maximal when the conductivity mismatch is large and the particle is close to the bottom wall. In Fig. 13, we present the asymptotic solution for weak confinement, $\delta_w \gg 1$.

5 Conclusion

We calculate the electric force on a spherical colloid between two planar surfaces in the presence of a uniform electric field. We consider the general case of the colloid and the suspending media that have arbitrary conductivities. We employ the leaky dielectric model, which assumes bulk media to be charge neutral (and thus electrostatic potential satisfying Laplace equation) and continuous normal current across the particle-medium interface. The charge carried by conduction accumulates at the particle surface and gives rise to free-charge polarization of the particle. We construct a general solution

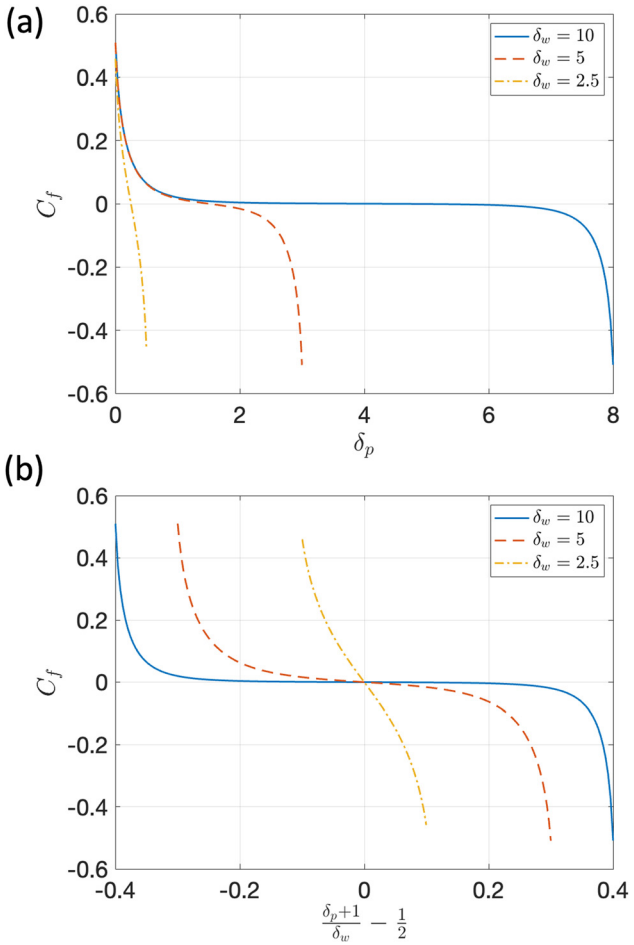

Fig. 8 Tangential field: force coefficient C_f as a function of the dimensionless particle to bottom wall gap sizes δ_p, or the normalized gap size, $(\delta_p + 1)/\delta_w - 1/2$, for various δ_w. χ = 0.2.

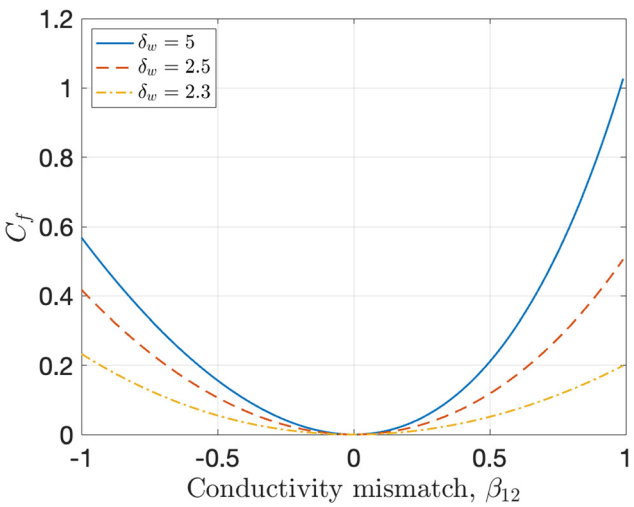

Fig. 9 Tangential field: force coefficient C_f as a function of the dimensionless conductivity mismatch β12 for various δ_w. δ_p = 0.1.

for the electric potential is using the method of images. The force on the particle is calculated using the effective multipole

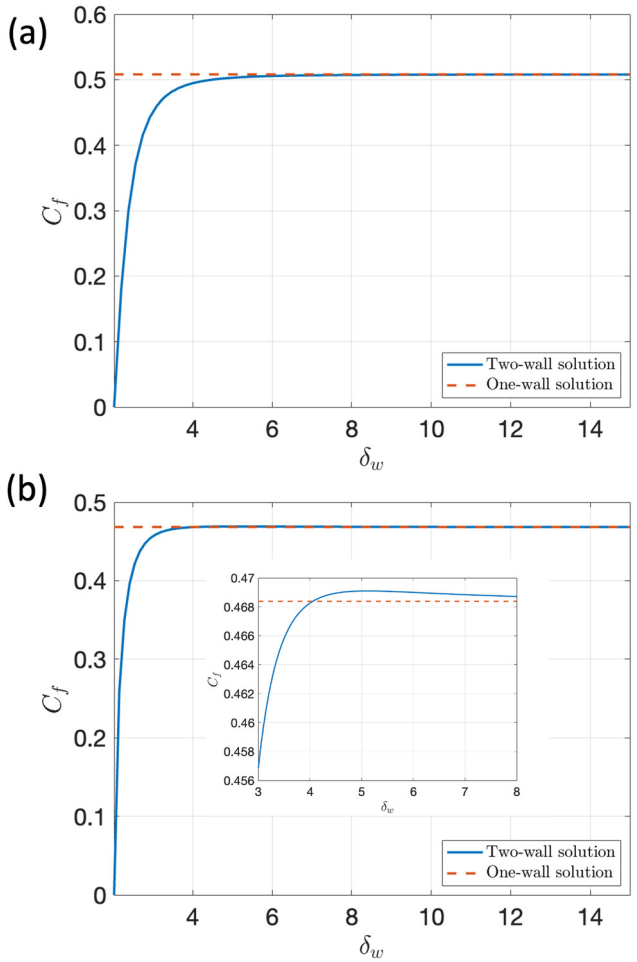

Fig. 10 Tangential field: force coefficient C_f as a function of the Dimensionless distance between the two walls δ_w. (a) δ_p = 0.01, and χ = 5 (b) δ_p = 0.01, and χ = 0.2.

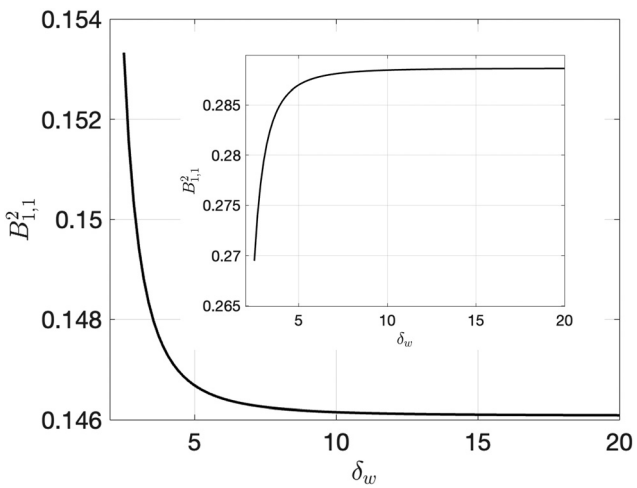

Fig. 11 Tangential field: the square of dimensionless dipole, $B_{1,1}$, as a function of dimensionless confinement δ_w for χ = 0.2 and δ_p = 0.01. Inset: χ = 5, δ_p = 0.01.

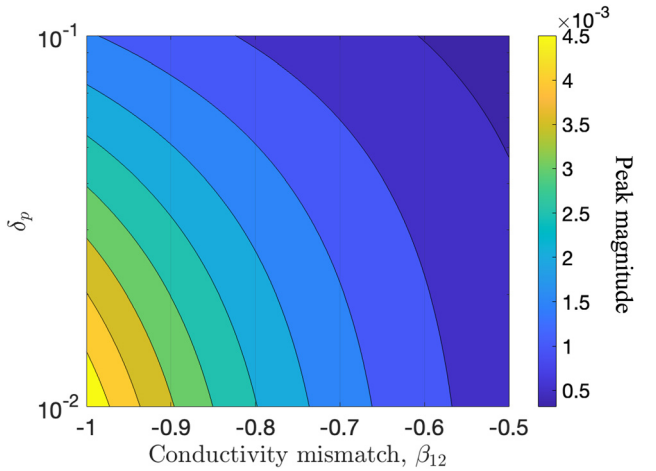

Fig. 12 Tangential field: peak magnitude of the force coefficient, scaled by the one wall solution, as a function of the conductivity mismatch β_{12} and δ_p.

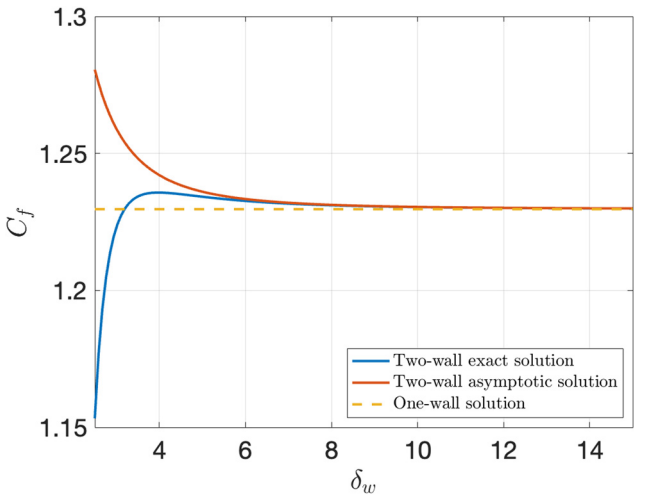

Fig. 13 Tangential field: force coefficient C_f as a function of the distance between the two planes, compared to the asymptotic solution. δ_p = 0.01, χ = 0.

method. We find that the particle is attracted by the closer boundary in the case of normal electric field, and repelled in the case of tangential electric field. The calculation also shows that while in general the top wall weakens the interaction, the force on the particle could exceed the one-wall problem when $\sigma_1 > \sigma_2$ (particle more conducting than the suspending medium) in the case of an electric field applied normal to the boundaries, and $\sigma_1 < \sigma_2$ for a tangentially applied electric field. Our findings will be useful for the design micro-electro-mechanical systems to manipulate particles such as colloids, droplets, and biological cells with electric fields.

Conflicts of interest

There are no conflicts to declare.

Appendices

Appendix A: A conducting sphere between two electrodes

In this case, the particle surface is equipotential and the boundary condition at $r = 1$ becomes $\Phi_2 = \Phi_p$. The electric potential outside the particle is

$$\Phi_2 = \sum_{n=0}^{\infty} \left(\frac{B_{n,0}}{r^{n+1}} + M'_{n,0} r^n \right) P_n(\cos\theta). \tag{40}$$

where $M'_{0,0} = M_{0,0} - \delta_c$ and the $M'_{n,0}$ are given by eqn (26). The multipoles $B_{l,0}$ are solutions of

$$\sum_{l=0}^{\infty} \left(N^{(0)}_{n,l} + \delta_{nl} \right) B_{l,0} = G_{n,0},$$

with $G_{n,0}$ being

$$G_{n,0} = \begin{cases} \Phi_P + \delta_c & n = 0, \\ 1 & n = 1, \\ 0 & n \geq 2. \end{cases} \tag{41}$$

The dimensionless net charge on the particle, scaled by $\varepsilon_2 E_0 a^2$ is

$$Q = -\oint_{r=1} \frac{\partial \Phi_2}{\partial r} \mathrm{d}S = 4\pi B_0. \tag{42}$$

The electric force on the particle is calculated by integrating the Maxwell stress tensor on the particle surface,

$$C_f = \oint_{r=1} \mathbf{e}_z \cdot \mathbf{T}_2 \cdot \mathbf{e}_r \mathrm{d}S, \tag{43}$$

where

$$\mathbf{T}_2 = \left[\mathbf{E}_2 \mathbf{E}_2 - \frac{1}{2} (\mathbf{E}_2 \cdot \mathbf{E}_2) \mathbf{I} \right]. \tag{44}$$

The integral is evaluated analytically,

$$C_f = 4\pi \sum_{n=0}^{\infty} \frac{n+1}{(2n+1)(2n+3)} L_n L_{n+1}, \tag{45}$$

where L_n is

$$L_n = -(n+1) B_{n,0} + n M'_{n,0}. \tag{46}$$

Acknowledgements

This work was supported by NSF award DMS-2108502.

Notes and references

1 D. C. Prieve, P. J. Sides and C. L. Wirth, *Curr. Opin. Colloid Interface Sci.*, 2010, **15**, 160–174.
2 O. D. Velev and K. H. Bhatt, *Soft Matter*, 2006, **2**, 738–750.
3 A. Van Blaaderen, M. Dijkstra, R. van Roij, A. Imhof, M. Kamp, B. Kwaadgras, T. Vissers and B. Liu, *Eur. Phys. J.: Spec. Top.*, 2013, **222**, 2895–2909.
4 T. D. Edwards and M. A. Bevan, *Langmuir*, 2014, **30**, 10793–10803.
5 B. Bharti and O. D. Velev, *Langmuir*, 2015, **31**, 7897–7908.
6 A. A. Harraq, B. D. Choudhury and B. Bharti, *Langmuir*, 2022, **38**, 3001–3016.
7 P. M. Vlahovska, *Annu. Rev. Fluid Mech.*, 2019, **51**, 305–330.
8 J. M. Montanero and A. M. Gañán-Calvo, *Rep. Prog. Phys.*, 2020, **83**, 097001.
9 W. D. Ristenpart, I. A. Aksay and D. A. Saville, *Phys. Rev. Lett.*, 2003, **90**, 128303.
10 J. Yan, M. Han, J. Zhang, C. Xu, E. Luijten and S. Granick, *Nat. Mater.*, 2016, **15**, 1095.
11 K. Han, C. W. Shields IV and O. D. Velev, *Adv. Funct. Mater.*, 2018, **28**, 1705953.
12 M. Driscoll and B. Delmotte, *Curr. Opin. Colloid Interface Sci.*, 2019, **40**, 42–57.
13 N. M. Diwakar, G. Kunti, T. Miloh, G. Yossifon and O. D. Velev, *Curr. Opin. Colloid Interface Sci.*, 2022, 101586.
14 A. Boymelgreen, J. Schiffbauer, B. Khusid and G. Yossifon, *Curr. Opin. Colloid Interface Sci.*, 2022, 101603.
15 S. Gangwal, O. J. Cayre, M. Z. Bazant and O. D. Velev, *Phys. Rev. Lett.*, 2008, **100**, 058302.
16 F. Ma, X. Yang, H. Zhao and N. Wu, *Phys. Rev. Lett.*, 2015, **115**, 208302.
17 D. Nishiguchi and M. Sano, *Phys. Rev. E: Stat., Nonlinear, Soft Matter Phys.*, 2015, **92**, 052309.
18 A. Bricard, J.-B. Caussin, N. Desreumaux, O. Dauchot and D. Bartolo, *Nature*, 2013, **503**, 95–98.
19 A. Bricard, J.-B. Caussin, D. Das, C. Savoie, V. Chikkadi, K. Shitara, O. Chepizhko, F. Peruani, D. Saintillan and D. Bartolo, *Nat. Commun.*, 2015, **6**, 7470.
20 A. Snezhko, *Curr. Opin. Coloid Interface Sci.*, 2016, **21**, 65–75.
21 H. Karani, G. E. Pradillo and P. M. Vlahovska, *Phys. Rev. Lett.*, 2019, **123**, 208002.
22 G. E. Pradillo, H. Karani and P. M. Vlahovska, *Soft Matter*, 2019, **15**, 6564–6570.
23 B. Zhang, H. Karani, P. M. Vlahovska and A. Snezhko, *Soft Matter*, 2021, **17**, 4818–4825.
24 H. A. Stone, A. D. Stroock and A. Ajdari, *Annu. Rev. Fluid Mech.*, 2005, **36**, 381–411.
25 J. Wu, W. Wen and P. Sheng, *Soft Matter*, 2012, **8**, 11589–11599.
26 P. Zhu and L. Wang, *Lab Chip*, 2017, **17**, 34–75.
27 A. T. Pérez, *J. Electrost.*, 2002, **56**, 199–217.
28 A. M. Drews, M. Kowalik and K. J. Bishop, *J. Appl. Phys.*, 2014, **116**, 074903.
29 M. H. Davis, *Q. J. Mech. Appl. Math.*, 1964, **17**, 499–511.
30 W. Lin, *J. Electromagn. Waves Appl.*, 1994, **8**, 195–203.
31 C. Xiaoping, *J. Electrost.*, 1987, **19**, 201–204.
32 K. Danov, P. Kralchevsky, K. Ananthapadmanabhan and A. Lips, *Langmuir*, 2006, **22**, 106–115.
33 R. D. Stoy, *J. Appl. Phys.*, 1989, **65**, 2611–2615.
34 A. T. Pérez and R. Fernández-Mateo, *J. Electrost.*, 2021, **112**, 103601.

35 M. Washizu and T. B. Jones, *IEEE Trans. Ind. Appl.*, 1996, **32**, 233–242.
36 E. Yariv, *Phys. Fluids*, 2006, **18**, 031702.
37 J. Melcher and G. Taylor, *Annu. Rev. Fluid Mech.*, 1969, **1**, 111–146.
38 G. I. Taylor, *Proc. R. Soc. London, Ser. A*, 1966, **291**, 159–166.
39 Z. Wang, M. J. Miksis and P. M. Vlahovska, *Phys. Rev. E*, 2022, **106**, 034607.
40 D. A. Saville, *Annu. Rev. Fluid Mech.*, 1997, **29**, 27–64.
41 O. Schnitzer and E. Yariv, *J. Fluid Mech.*, 2015, **773**, 1–33.
42 Y. Mori and Y.-N. Young, *J. Fluid Mech.*, 2018, **855**, 67–130.
43 P. Marthaler, A. Class, Y. Mori and Y.-N. Young, *J. Fluid Mech.*, 2023, **962**, E1.
44 M. Ma, M. R. Booty and M. Siegel, *J. Fluid Mech.*, 2022, **943**, A47.
45 J. López-Herrera, M. Herrada and A. Gañán-Calvo, *J. Fluid Mech.*, 2023, **964**, A19.
46 M. Washizu and T. B. Jones, *IEEE Trans. Ind. Appl.*, 1996, **32**, 233–242.

